npj | clean water

www.nature.com/npjcleanwater

ARTICLE OPEN

Kirigami fog nets: how strips improve water collection

Pierre-Brice Bintein[1,2]✉, Axel Cornu[1,2], Floriane Weyer[3], Nicolas De Coster[2,4], Nicolas Vandewalle[3] and Denis Terwagne[1,2]✉

As scarcity of water is expected to intensify with global warming, unconventional water sources such as advective fogs may become essential. In numerous arid regions, nets are used to harvest such water droplets. However, many current fog nets are either not durable or expensive, and have poor performances for short time or low intensity fog events. With a dedicated test bench, we show here that a low-cost net with kirigami design offers a higher and faster fog collecting ability than the usual fibers nets. This kirigami fog net consists of a continuous network of strips where water quickly forms a stable film, accounting for its superior capture efficiency. We rationalize this mechanism with a simplified structure composed of disconnected strips whose optimization paves the way to the shaping of original fog nets such as the kirigami one.

npj Clean Water (2023)6:54 ; https://doi.org/10.1038/s41545-023-00266-6

INTRODUCTION

The growing water scarcity is one of the main global challenges[1]: around four billion people currently face severe lack of water for at least one month per year[2], and an exacerbation by climate change is expected[3], with more than half of the world's population living in water-stressed regions by 2050[4]. Atmospheric moisture harvesting is part of the water resources that can locally complement the conventional ones[5–10]. More specifically, fog water collection combines the advantages of being a passive, low-cost, low-maintenance, sustainable and community-scale technique; it often involves participatory projects with lower economical and ecological costs than massive water infrastructures[11,12]. Such a water supply has long been known[13–15] and nets are already used in arid or semi-arid areas where advective fog is abundant[16,17].

Yet producing affordable, efficient and durable fog nets is a remaining challenge: easily accessible low-cost nets as the "Raschel mesh" (from grocery packing)[16,18] have low efficiency and can break in high winds[19,20]. Previous studies tested new geometries together with the use of coatings to improve drainage as on Raschel mesh[21], grids[22] and cylinders[23]; "fog harps" made of vertical wires have also shown good drainage and partial avoidance of clogging[24–28]. Kirigamis (made of cut surfaces) have been recently exploited either in 2D geometry with small tapered obstacles directing droplets[29,30] or in 3D with large folded plates rectifying the flow[31]. 3D structures show higher robustness and efficiency[32–34], while multi-layered collectors can overcome the performances of single nets[35–39]. But such prototypes are sometimes fragile (when chemically coated or exposed to harsh environments) and costly (with heavy or elaborate materials). Furthermore, comparing them quantitatively remains elusive as they are often individually tested either in confined laboratory set-ups with specific flow circumvention, or on the field with variable wind velocity, liquid water content and drop size distribution. The influence of these interdependent parameters on the efficiency of standard fog nets is complex[40], and the few field comparisons with new meshes hardly show a significant improvement[34,41]. Besides, the time evolution of net performances is rarely measured despite the importance of transient underlined in field studies[40,41]; a stationary efficiency is even not achieved under light fog conditions.

Here we built a dedicated test bench (sketched in Fig. 1) allowing to measure and compare the dynamic efficiencies of different nets under the same fog flow, defined by its adjustable velocity U and flux q (as detailed in the Supplementary Information), to follow their temporal evolution and to distinguish between the different mechanisms involved in fog collection. The global fog harvesting efficiency η of a single-layer net results from three processes usually assumed to be independent: η is the product of the aerodynamic, capture and drainage efficiencies[42,43]. We first recall these mechanisms and indicate how to characterize them with our setup. The aerodynamic efficiency η_{aero} reflects the circumvention of air around the whole net: the filtered proportion of the incoming flow is the ratio between the cross section S_o of the stream tube far upward the obstacle and the unperturbed section S which is the projection of the net area; from this one, only the solid fraction called the solidity (or shade coefficient) and denoted as s can collect water, so that $\eta_{aero} = (S_o/S)s = (U_{net}/U)s$[42]. This latter expression (where U_{net} denotes the air velocity through the net) results from flux conservation and allows to determine η_{aero} for a given configuration: here an anemometer measures the air velocities with (U_{net}) and without (U) the net. As the ratio U_{net}/U is a decreasing function of s, η_{aero} shows a maximum at an intermediate value of solidity[42]. The capture of fog droplets with typical sizes 1–50 µm mainly results from their inertia, which prevents them from following the curved streamlines at the vicinity of obstacles. This impaction mechanism is characterized by the Stokes number St, the ratio of the stopping distance of a drop (with radius r and density ρ) by Stokes friction in air (with velocity U and viscosity μ_a) over the width D of the obstacle: $St = 2\rho U r^2/9\mu_a D$[44]. The capture efficiency η_{capt} is described as an increasing function of St[44,45] so that thin obstacles are individually more efficient to catch fog. However, the corresponding net with predefined s easily presents openings, when they are small, clogged by water[22], resulting in non-optimal effective solidities and larger equivalent obstacles so that both η_{aero} and η_{capt} are reduced. In addition to the deviation of small drops around obstacles, bigger ones may bounce rather than stick to them, also lowering η_{capt}. Usual hydrophilic materials avoid such rebounds, but their adhesion hinder the flow of caught water along the net down to a gutter; the drainage efficiency η_{drain}

[1]Frugal Lab, Faculté des Sciences, Université Libre de Bruxelles (ULB), 1050 Brussels, Belgium. [2]Fab Lab ULB, Université Libre de Bruxelles (ULB), 1050 Brussels, Belgium. [3]GRASP, Faculté des Sciences, University of Liège (ULiège), 4000 Liège, Belgium. [4]Institut Royal Météorologique (IRM), 1180 Brussels, Belgium. ✉email: pierre-brice.bintein@u-paris.fr; Denis.Terwagne@ulb.be

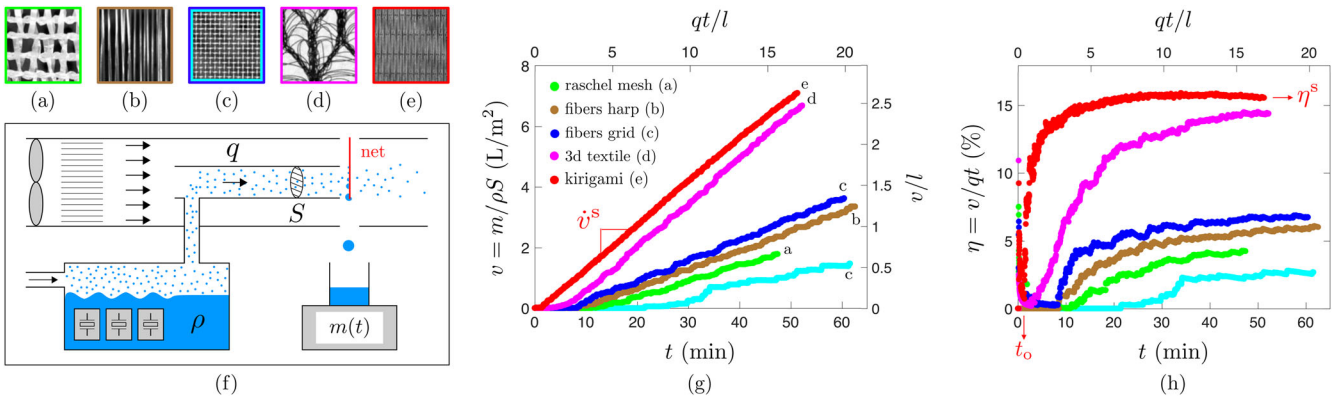

Fig. 1 Comparison between dynamic efficiencies of several fog nets. a–e Pictures (with size 2 x 2 cm^2) of the tested nets: (**a**) Raschel mesh (width $D = 1.5$ mm and solidity $s \approx 74\%$), (**b**) harp of nylon fibers ($D = 500$ µm, $s \approx 50\%$), (**c**) grid of stainless steel fibers ($D = 406$ µm, $s = 54\%$), (**d**) 3D textile (®Cloudfisher) ($D \approx 130$ µm, $s \approx 54\%$), (**e**) kirigami fog net ($D \approx 550$ µm, $s \approx 66\%$). **f** Schematic of the experimental setup to measure dynamic efficiencies at fixed wind velocity U and fog flux q. **g** Collected water volume per unit of net exposed area S as a function of time t, for the different nets (metallic grid is either bare, dark blue, or sprayed with Ultra Ever Dry superhydrophobic coating, light blue) under the same fog conditions ($U = 1.5$ m/s, $q \approx 15$ µm/s, $LWC \approx 10$ g/m^3). Dimensionless coordinates are the emitted qt and collected v water heights divided by the capillary length l. **h** Dynamic efficiencies of the nets $\eta = v/qt$ as a function of time. t_o is the onset time of collection and η^s is the stationary efficiency.

combines this effect with the potential re-entrainment of captured droplets in the flow. In our setup, two weighing scales measure the masses of the harvested water fallen from the net in the gutter (m) and of the captured water remaining on it (m_{net}), so that the drainage efficiency can be measured as $\eta_{drain} = m/(m_{net} + m)$. Then the experimental capture efficiency is deduced from $\eta_{capt} = \eta/\eta_{aero}\eta_{drain}$.

RESULTS AND DISCUSSION

Superiority of kirigami fog net over usual nets

Figure 1 first compares the global efficiencies of some of the existing nets with optimized geometries (pictured in Fig. 1a–e): a 2-layer Raschel mesh[18], a harp of fibers[24], a grid of fibers[22] and a 3D textile designed for fog recuperation[32]. We add measurements with our original optimized kirigami fog net; the kirigami pattern of parallel slits is made by cutting a 60-micrometers thick polypropylene sheet with a laser cutting machine. All nets are cut into the same rectangular shape (with area 9×18 cm^2) and placed inside the test bench; precisions on the nets, their optimization and the protocol are given in the Methods section. We fix the fog speed $U = 1.5$ m/s and the fog flow per surface unit $q = \dot{m}_o/\rho S = 15$ µm/s (where m_o is the mass of the water tank). The liquid water content is then $LWC = \rho q/U \approx 10$ g/m^3, which is 30 to 130 times higher than the natural ones[45], allowing us to reach stationary states earlier. The recovered water masses m are normalized by the water density ρ times the area S of the incoming flow to get the water volumes v harvested by surface unit of the nets (or the equivalent water heights). Figure 1g presents v as a function of time t. After a variable delay (up to tens of minutes) corresponding roughly to the time required for the hung water mass to stabilize around a constant value (plotted in Supplementary Fig. 1 in the Supplementary Information), the nets are in stationary states defined by constant slopes $\dot{v}^s$: the additional collected droplets compensate the water falling by gravity in the tank. Two main groups can be distinguished: the Raschel mesh (a) and the simple fiber meshes (b,c) behave similarly, with a harvesting velocity $\dot{v}^s \approx 1$ µm/s, whereas the 3D textile (d) and the kirigami (e) have close higher $\dot{v}^s \approx 2.4$ µm/s. Such an improvement is expected for the optimized shape of 3D textile (with small fibers to increase capture, and almost no horizontal parts to increase drainage) as previously measured during field collection[34]. More surprisingly, our optimized kirigami net is the most efficient of the set; it even outperforms the 3D textile because of an earlier water harvest: even with a slightly smaller rate of collection, it still collects more water in case of fog events (with similar high q) lasting for less than an hour. The upper and right axis of Fig. 1g correspond to dimensionless data with the emitted (qt) and collected (v) equivalent water heights divided by the capillary length $l = (\gamma/\rho g)^{1/2} = 2.7$ mm at the nebulized water temperature of 30 °C (where g and γ denote gravity and the surface tension of water), allowing possible comparison between different fog conditions (via q) and collected liquids (via l). The fog flux q slightly influences the hierarchy of Fig. 1g, with a higher q leading to smaller differences between nets performances (as seen in Supplementary Figs. 2 and 3 in the Supplementary Information). This ranking is further evidenced by plotting, in Fig. 1h, the dynamic efficiencies of the nets $\eta = v/qt$ as a function of time. Whereas the efficiencies of usual nets are delayed and slowly increase to stabilize after about 1 hour, the kirigami efficiency increases suddenly, with the lower onset time of water harvesting t_o (a few seconds), to quickly reach (after 10–20 min) the higher stationary efficiency η^s (around 15%), with an almost step profile. Such a net might thus be able to efficiently harvest water during very short time fog events. Note that a small t_o is linked to a high η^s; thereafter, we use η^s to characterize the nets, with $\eta^s \simeq \dot{v}^s/q$ in a good approximation.

Qualitative explanation of kirigami fog net efficiency

To elucidate the good dynamical harvesting capacities of kirigami fog nets, we first show, in Fig. 2a, shots of such a net from the beginning of fog exposition up to the detachment of the first drop (see full movie in Supplementary Movie 1). Whereas water accumulates at the bottom of the net by forming big hanging drops growing and eventually falling, the whole upper part of the net appears to be surprisingly free of drops. Magnification (red-circled zoom-ins) reveals the quick formation of a water film by capture and coalescence of small impacting droplets: after some seconds, these droplets (dark speckles appearing on the 4s zoom-in) are not observable anymore, and the formed film gets a stationary shape in a few tenths of seconds, with a thickness h fixed by a dynamic equilibrium between impinging droplets and water drainage (here $h \approx 0.25$ mm measured from the Supplementary Fig. 1 in the Supplementary Information). The presence of water becomes only perceptible through the slight curvature of

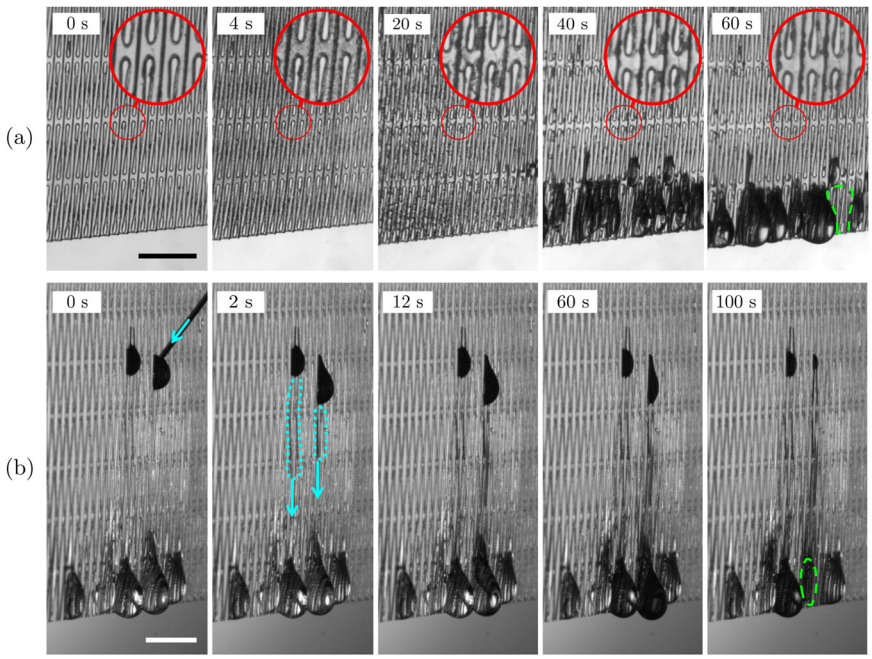

Fig. 2 Visualizations of water repartition on a kirigami fog net (same net and fog conditions as in Fig. 1e). a On a dry fog net (appearing transparent on the first magnified red circle) exposed during one minute to fog flow, the captured fog droplets (discernible as dark speckles at 4 s by magnification) coalesce to form bigger drops (20 s) evolving into a water film (40 s) which is stationary and visible through its curvature (comparing with the dry net). This film quickly covers the whole net and catches the oncoming droplets, while continuously draining under gravity; water accumulates into big drops growing at the bottom of the net and eventually falling (60 s), leaving an empty area (enclosed by a dashed green line in the bottom right corner). **b** Out of the fog flow, the remaining water film can be evidenced by depositing drops of darkened water from a syringe needle (0 s), with water motion underlined by blue arrows. These drops remain pinned at kirigami edges, but are drained through the water film (as highlighted with dotted blue lines at 2 s) toward bigger drops with lower capillary pressure, which grow and darken before detaching. Scale bars indicate 5 mm.

this film. To reveal the liquid transport through the film, we then stop the fog flow and use a syringe to deposit drops of water darkened with food coloring on the net. The pictures on Fig. 2b show that these drops stay pinned at the edges of the strips (where contact angle hysteresis overcomes gravity) but shrink by emptying into drops located at the bottom through the pre-established film, as revealed by dark vertical paths slightly wider than the colored drops; the flow is preferentially downwards but widens with time by diffusion (see full movie in Supplementary Movie 2). The film occupies the whole net, and lateral connections may ensure robustness of flow despite potential obstacles (as small defects or dust) in the net. The early existence of a stable water film covering the kirigami net allows a qualitative explanation of its superior efficiency: whereas its cross-section is almost unchanged, so that clogging is avoided and η_{aero} remains optimal, its surface state is rendered perfectly wet which might reduce significantly rebounds on and detachment from the solid, so that η_{capt} is increased; besides, as the excess of water is sliding on a lower water layer, the friction is reduced compared to sliding over a solid[46], so that η_{drain} is maximal. Thus, the stability of such film is essential for good harvesting performances; here we comparatively discuss this stability on strips and fibers, without considering the airflow effects assumed to be negligible for usual wind intensities[47,48]. Gravity-driven liquid filaments of dynamic viscosity μ and velocity V are known to be stable on flat hydrophilic surfaces for small capillary numbers $Ca = \mu V/\gamma$; they start emitting drops above $Ca \approx 0.2$[49]. In the experimental conditions of Fig. 1, the water velocity is given by $\dot{v}^s$ so that Ca is on the order of 10^{-8}, way below 0.2. We expect the film to remain stable under common lighter fog field conditions associated with even smaller capillary numbers. Note that such films have been partially observed on Raschel mesh, which might explain its good performances on field despite any advanced optimization of its strips[41]. On fiber-made nets, liquid films usually undergo the Rayleigh-Plateau instability, evolving quickly into droplets (connected by a thin unstable film). Yet flow advection may lead to a nonlinear saturation of this instability: the film is maintained by large amplitude waves when its thickness h is lower than a critical value[50,51]. For the harp of fibers we used (Fig. 1, $D = 500$ µm), $h_c \approx 3.6$ µm, way below the estimated thickness of an hypothetic uniform film deduced from weighting (in the Supplementary Fig. 1 of the Supplementary Information), around 1 mm, for which any fiber thiner than 3.2 mm won't stabilize the film. Such threshold is not expected to vary with fog flow as long as $D < 0.2\, l_c \approx 540$ µm[52], so that all the thin fibers usually deployed to catch fog will lead to film destabilization into droplets. Again, this has disadvantages for each efficiency component: droplets will flow only once gravity forces overcome the capillary adhesion forces, hindering drainage efficiency; the section of the net is evolving with time[25], which compromises its aerodynamics optimization and can even cause clogging; and the impinging drops must catch bigger (liquid) obstacles or solid parts, both less favorable to capture.

Quantitative optimization of harps of strips

To isolate the key features of fog collecting with strips and precise quantitatively their advantages over fibers, we measure the efficiencies of simplified nets made of non entangled vertical obstacles (so called 'harps') that are either cylindrical fibers or flat strips (Fig. 3a). Several studies have been devoted to harps of fibers[24–28]; here we built three of them made of copper fibers with different diameters (0.5, 1 and 2 mm), together with harps of flat laser-cut mylar strips ($D = 0.5$–8 mm, so that the Stokes number varies from 0.125 to 2 in our experimental conditions). All of these

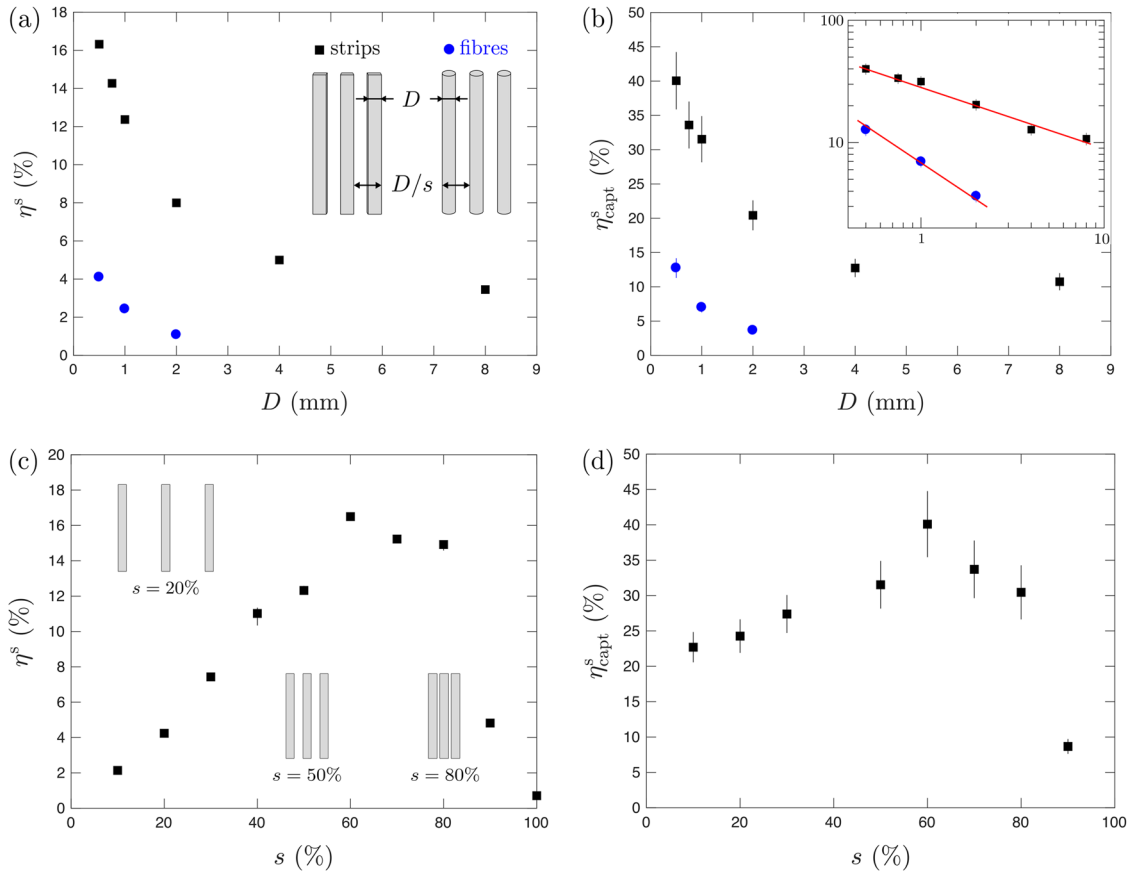

Fig. 3 Stationary efficiencies of fog harps. a Stationary efficiencies η^s and (**b**) stationary capture efficiencies η^s_{capt} for harps of strips or fibers, varying the size D of obstacles, for a fixed solidity $s = 50\%$. Insert in (**a**): definition of D and s; insert in (**b**): same data in logarithmic scales show different scalings with red lines of slopes $-1/2$ and -1. (**c**, **d**) Evolution of these efficiencies with the solidity s for harps of strips with $D = 1$ mm. Error bars in (**a**, **c**) originating from uncertainty measurements and variability are mostly smaller than symbol size whereas error bars in (**b**, **d**) mainly account for the gap in U_{net} when measured upstream or downstream sides of the net.

nets have the same area (of $6 \times 6\text{cm}^2$) and solidity $s = 50\%$ (that is, close to the optimal value for fibers[42].) When fixed on the same support and exposed to the same flow, harps of strips outperform the fibers ones with a stationary efficiency 4 to 8 times higher (Fig. 3a), that is, even more broadly than in Fig. 1. As for fiber nets, larger obstacles deflect more the flow, thus collecting less droplets. We decompose the contributions to water harvesting by measuring the aerodynamic and drainage efficiencies (plotted in the Supplementary Figs. 4 and 5 in the Supplementary Information). η_{aero} is roughly constant and independent of D, as expected for fibers at fixed s[42]; this feature is recovered for strips. The drainage efficiencies η_{drain} appear to be constant after a transitional regime, which is shorter for strips than for fibers, and roughly independent of D and s. Both η_{aero} and η_{drain} are slightly higher for strips, yet cannot account for the gap of Fig. 3a. We then plot the dynamic capture efficiencies $\eta_{capt} = \eta/\eta_{drain}\eta_{aero}$ as a function of time (Supplementary Fig. 5 in the Supplementary Information); their stationary values are presented in Fig. 3b which shows that the main improvement of strips compared to fibers lies in their capturing abilities. Such difference was already observed for aerosol impaction on single elements[53], yet less markedly; it may originate from the flow differences around circular and square cylinders, with higher recirculation length and drag coefficient for a square section[54]. Then drops are less following streamlines before an obstacle with sharp corners, and more recirculating after, which both promote their deposition; this latter is also probably affected by characteristics of the complex flow around strips, as the effect of viscous boundary layer, vortices (causing back-side impaction) and their shedding, as well as lift force[55–57], further complicated by interactions between neighboring strips[58,59]. These combined effects may explain the associated original power law of capture efficiency with the size of obstacle, with a halved exponent compared to fibers (as can be seen in the inserted logarithmic plot of Fig. 3b). η_{capt} for fibers harp roughly decreases as D^{-1} on the small tested range, which differs from the dependency with Stokes number calculated by Langmuir and Blodgett for an isolated cylinder, therefore only valid at low s[44]. Here ($s = 50\%$) interactions between nearby cylinders may lead to η_{capt} approximately proportional to St (thus D^{-1}) as measured for close wire geometries[36]; this scaling may reveal a regime where droplets lacking of inertia are intercepted by boundary layers[55,60]. For harps of strips, the smaller exponent might be due to a smaller local Stokes number (with no curvature and less centrifugal effects so that the influence of inertia is even reduced) leading to a correction depending on the Reynolds number of the fog flow around one strip $Re = \rho_a UD/\mu_a$ (with ρ_a the air density), varying between 50 and 800 in our experiments: $\eta_{capt} \propto StRe^{1/2}$[61], which gives a variation with the size of strips as $D^{-1/2}$ (and an approximately ten times higher order of magnitude), as seen in Fig. 3b. In practice, this slow decrease means that larger strips could also be used (for easier manufacturing or better mechanical properties) with a limited loss in efficiency. In addition, these good harvesting performances appears to be quite robust with no influence of the strip thickness and inclination angle on the stationary efficiency of the harp with fixed width ($D = 1$ mm) and solidity ($s = 50\%$) (as plotted in Supplementary Fig. 6). To further

optimize this harp of strips, we performed measurements with changing s from 10 to 100% at a constant $D = 1$ mm (Fig. 3c, d, Supplementary Figs. 4b and 7). The efficiency varies non-monotonously with the solidity: it is maximal for $s \approx 60\%$ and presents a plateau up to 80% before decreasing abruptly (Fig. 3c). A similar yet more symmetrical curve is theoretically expected for fibers net[42]; here the measured asymmetry may be due to blockage effects. Plotting the stationary capture efficiency in Fig. 3d allows removing such side effects (included in η_{aero}) and reveals the essential characteristics of the net that would presumably be maintened on field; as the remaining peak around $s = 60\%$ is less marked, an area of interest between 50 and 80% should be targeted. Such a large plateau is of practical interest as the effective solidity may vary depending on the net fabrication and holding procedures, as well as the stretchability of its material in the case of kirigami nets. Being just one sheet with cuts, a kirigami fog net not only benefits from the advantages of the strips, but is easier to manufacture and hold than a harp of strips. Besides, it is now flexible and can be either pre-stretched on a framework (to impose an optimal solidity, see Supplementary Fig. 8), deformed by the airflow (with a resulting curvature aerodynamically advantageous[42,43]) or both. Such flexibility is widely tunable with the cuts geometry[62]; it may help to withstand high winds and induce earlier fall of big hanging drops by light fluttering. Modifying the cut design to optimize the net shape for fog capture under different wind conditions defines a promising avenue for future work.

METHODS

Experimental test bench

The experimental set-up represented on Fig. 1f consists of 3 piezoelectric devices (Techsin DK-24 transducers vibrating at $F = 1.7$ MHz) that produce fine droplets when immersed into a tank of demineralized water to induce its ultra-sonic atomization[63,64]; the formed droplets are pushed by pressurized air into an inner tube of section $S = 22.5\ cm^2$, where the wind velocity U is imposed by a controlled fan. Here U can be varied between 0.5 and 2.5 m/s with a precision of 0.1 m/s. To produce a directional flow, two thin coaxial tubes with diameter 5 and 15 cm are used and placed in front of the fan and a laminarizer; this results into a fog flow rate q toward the net, which can be varied and calibrated by weighings of the water tank for different conditions (air velocity, pressurized air flow, number of piezoelectric devices turned on). Here q can be varied between 0 and 50 µm/s with a precision of 3 µm/s. The tested net (a typical kirigami sample is shown on Supplementary Fig. 9) is hanged to a precision scale (Sartorius LP1200S, 1 mg precision), not shown on the schematics, allowing to measure the collected mass m_{net} remaining hung on the net. Fog drops hit the net where they accumulate and coalesce until reaching a critical mass that detach by gravity: water eventually falls into a tank which mass m is recorded with time using another scale (VWR, 10 mg precision). Both scale signals are recorded on a computer with a homemade system. Note that each net is placed 1.5 cm away from the end of the tubes; in addition, another large coaxial tube is aligned 1.5 cm downstream of the net, which allows a directed fog flow that can still be deflected around the nets in some proportions. The induced blockage effect depends on the solidity of each net but is taken into account via the measured aerodynamic efficiency.

Calibration and experimental protocol

The fog emission is calibrated by weighing the water tank for several times which gives a mean mass diminution of the water tank per unit time $\dot{m}_o$; this rate is constant in a good approximation so that a constant fog flux is imposed for given conditions (number of piezoelectric devices switched on, mean height of water above the piezoelectric surface, air pressure, wind velocity). Note that we imposed fog emission during about 15 minutes before hanging a net to establish a relative humidity close to 100% in the inner tube so that evaporation of droplets is reduced. We measured the diameter of produced drops as $d \approx 10$ µm just above the transducers, in accordance with the dedicated study[65] describing the drop sizes by a two parameters Gamma distribution with extreme diameters on the order of 1 and 17 µm. Here, the few bigger drops recorded at the net location with a fast camera are around 50 µm in diameter, indicating probable coalescence between some droplets during their flight.

Tested nets. **Raschel mesh fog net** used in standard fog collectors consists in a double layer of woven polypropylene ribbons with $D = 1.5$ mm width, resulting in a solidity $s \approx 74\%$.

Harp of fibers are made of nylon fibers of diameter $D = 500$ µm, $s \approx 50\%$.

Grid of fibers are stainless steel fibers of diameter $D = 406$ µm, $s = 54\%$. These have been tested either bare or sprayed with Ultra Ever Dry superhydrophobic coating and corresponds, respectively, to the dark blue and light blue curves on Fig. 1g, h. Note that the low performances of superhydrophobic grids might be due to the more spherical shape of hanging droplets (before draining), that induce an important increase of the solidity.

3d textile (®Cloudfisher) is a spacer fabric designed for fog harvesting by ITV Denkendorf. It is made of polyethersulfone threads of diameter $D \approx 130$ µm, with $s \approx 54\%$. It is implemented in the Aqualonis FogCollectors (formerly known as the ®Cloudfisher) fog nets and is considered as one of the best fog net on the market. Already in use in different locations such as Morocco or the Canary Islands.

Kirigami fog net is a laser-cut (with laser cutting machine Epilog Laser MINI 24 60W) pre-stretched polypropylene sheet resulting in strips of width $D \approx 550$ µm with $s \approx 66\%$. Contact angles on such sheets where measured in the advancing $\theta_{adv} = 71 \pm 6°$ and receding $\theta_{rec} = 33 \pm 2°$ cases. The kirigami net is optimally stretched following measurements of fog harvesting with varying this stretching, as plotted in Supplementary Fig. 8. A global view of a typical mylar kirigami fog net sample, stretched or not, is shown in Supplementary Fig. 9.

Samples preparation

Sample nets, presented on Fig. 1, are all cut into 9 cm height-18 cm width rectangular nets, hanged (with a frame without lower side) to a scale and placed under controlled fog flow conditions thanks to a setup schematically shown in Fig. 1f (the upper scale is not shown on the schematic).

Harps materials and preparation

Harps of mylar (polyethylene terephthalate) strips have been made with laser-cut mylar strips hanged from laser-cut acrylic supports (with laser cutting machine Epilog Laser MINI 24 60W). Harps of copper fibers have been made with as-received copper wires hanged from similar laser-cut acrylic supports. Each harp (sketched on Fig. 3) has a size of $6 \times 6\ cm^2$ plus upper and bottom rigid edges to maintain their shapes in the flow. During experiments, they have been placed under fog for more than a hour with $U = 1.5$ m/s, $q \approx 15$ µm/s. Contact angles on planar materials where measured as $\theta_{adv} = 84 \pm 3°$ and $\theta_{rec} = 52 \pm 4°$ for copper, and $\theta_{adv} = 70 \pm 5°$ and $\theta_{rec} = 47 \pm 4°$ for mylar.

DATA AVAILABILITY

The data that support the findings of this study are available from the corresponding authors upon reasonable request.

Received: 15 November 2022; Accepted: 21 June 2023;
Published online: 20 July 2023

REFERENCES

1. United Nations Educational, Scientific and Cultural Organization. *United Nations World Water Development Report 2020: Water and Climate Change*. (UNESCO, Paris, 2020).
2. Mekonnen, M. M. & Hoekstra, A. Y. Four billion people facing severe water scarcity. *Sci. Adv.* **2**, e1500323 (2016).
3. Gosling, S. N. & Arnell, N. W. A global assessment of the impact of climate change on water scarcity. *Clim. Change* **134**, 371–385 (2016).
4. Kölbel, J., Strong, C., Noe, C. & Reig, P. *Mapping Public Water Management by Harmonizing and Sharing Corporate Water Risk Information*. https://www.wri.org/research/mapping-public-water-management-harmonizing-and-sharing-corporate-water-risk-information (2018).
5. Zhang, M., Liu, R. & Li, Y. Diversifying eater sources with atmospheric water harvesting to enhance water supply resilience. *Sustainability* **14**, 7783 (2022).
6. Wahlgren, R. V. Atmospheric water vapour processor designs for potable water production: a review. *Water Res.* **35**, 1–22 (2001).
7. Kim, H. et al. Adsorption-based atmospheric water harvesting device for arid climates. *Nat. Commun.* **9**, 1–8 (2018).
8. Fathieh, F. et al. Practical water production from desert air. *Sci. Adv.* **4**, eaat3198 (2018).
9. Lekouch, I. et al. Dew, fog, and rain as supplementary sources of water in south-western Morocco. *Energy* **36**, 2257–2265 (2011).
10. Kaseke, K. F. & Wang, L. Fog and dew as potable water resources: maximizing harvesting potential and water quality concerns. *GeoHealth* **2**, 327–332 (2018).
11. Gleick, P. H. Global freshwater resources: soft-path solutions for the 21st century. *Science* **302**, 1524–1528 (2003).
12. Qadir, M., Jiménez, G. C., Farnum, R. L., Dodson, L. L. & Smakhtin, V. Fog water collection: challenges beyond technology. *Water* **10**, 372 (2018).
13. Went, F. W. Fog, mist, dew and other sources of water. in *The Yearbook of Agriculture: Water* (ed. Stefferud, A.) 103–109 (The United States Department of Agriculture, Washington, 1955).
14. Marzol-Jaén, M. V. in *Tropical Montane Cloud Forests: Science for Conservation and Management* (eds. Bruijnzeel, L. A., Scatena, F. N. & Hamilton, L. S.) 352–358 (Cambridge University Press, Cambridge, 2011).
15. Gultepe, I. et al. Fog research: a review of past achievements and future perspectives. *Pure Appl. Geophys.* **164**, 1121–1159 (2007).
16. Klemm, O. et al. Fog as a fresh-water resource: overview and perspectives. *AMBIO* **41**, 221–234 (2012).
17. Fessehaye, M. et al. Fog-water collection for community use. *Renew. Sust. Energy Rev.* **29**, 52–62 (2014).
18. Schemenauer, R. S. & Cereceda, P. A proposed standard fog collector for use in high-elevation regions. *J. Appl. Meteorol. Climatol.* **33**, 1313–1322 (1994).
19. Holmes, R., Rivera, Jd. D. & de la Jara, E. Large fog collectors: new strategies for collection efficiency and structural response to wind pressure. *Atmos. Res.* **151**, 236–249 (2015).
20. Rivera, Jd. D. & Lopez-Garcia, D. Mechanical characteristics of Raschel mesh and their application to the design of large fog collectors. *Atmos. Res.* **151**, 250–258 (2015).
21. Rajaram, M., Heng, X., Oza, M. & Luo, C. Enhancement of fog-collection efficiency of a Raschel mesh using surface coatings and local geometric changes. *Colloids Surf. A: Physicochem. Eng. Asp.* **508**, 218–229 (2016).
22. Park, K.-C., Chhatre, S. S., Srinivasan, S., Cohen, R. E. & McKinley, G. H. Optimal design of permeable fiber network structures for fog harvesting. *Langmuir* **29**, 13269–13277 (2013).
23. Seo, D., Lee, J., Lee, C. & Nam, Y. The effects of surface wettability on the fog and dew moisture harvesting performance on tubular surfaces. *Sci. Rep.***6**, 24276 (2016).
24. Shi, W., Anderson, M. J., Tulkoff, J. B., Kennedy, B. S. & Boreyko, J. B. Fog harvesting with harps. *ACS Appl. Mater. Interfaces* **10**, 11979–11986 (2018).
25. Labbé, R. & Duprat, C. Capturing aerosol droplets with fibers. *Soft Matter.* **15**, 6946–6951 (2019).
26. Jiang, Y., Savarirayan, S., Yao, Y. & Park, K.-C. Fog collection on a superhydrophilic wire. *Appl. Phys. Lett.* **114**, 083701 (2019).
27. Shi, W., van der Sloot, T. W., Hart, B. J., Kennedy, B. S. & Boreyko, J. B. Harps enable water harvesting under light fog conditions. *Adv. Sust. Syst.* **4**, 2000040 (2020).
28. Kowalski, N. G., Shi, W., Kennedy, B. S. & Boreyko, J. B. Optimizing fog harps. *ACS Appl. Mater. Interfaces* **13**, 38826–38834 (2021).
29. Bai, H. et al. Cactus kirigami for efficient fog harvesting: simplifying a 3d cactus into 2d paper art. *J. Mater. Chem. A* **8**, 13452–13458 (2020).
30. Yu, Z. et al. Bio-inspired copper kirigami motifs leading to a 2D-3D switchable structure for programmable fog harvesting and water retention. *Adv. Funct. Mater.* **33**, 2210730 (2023).
31. Li, J. et al. Aerodynamics-assisted, efficient and scalable kirigami fog collectors. *Nat. Commun.* **12**, 1–8 (2021).
32. Sarsour, J., Stegmaier, T., Linke, M. & Planck, H. Bionic development of textile materials for harvesting water from fog. In *Proc. 5th International Conference on Fog, Fog Collection and Dew* 248–251 (FOGDEW, 2010).
33. Feld, S. I., Spencer, B. R. & Bolton, S. M. Improved fog collection using Turf reinforcement mats. *J. Sust. Water Built Environ.* **2**, 04016002 (2016).
34. Schunk, C. et al. Testing water yield, efficiency of different meshes and water quality with a novel fog collector for high wind speeds. *Aerosol. Air Qual. Res.* **18**, 240–253 (2018).
35. Demoz, B. B., Collett Jr, J. L. & Daube Jr, B. C. On the Caltech active strand cloudwater collectors. *Atmos. Res.* **41**, 47–62 (1996).
36. Brunazzi, E. & Paglianti, A. Design of complex wire-mesh mist eliminators. *AIChE J.* **46**, 1131–1137 (2000).
37. Regalado, C. M. & Ritter, A. The design of an optimal fog water collector: a theoretical analysis. *Atmosp. Res.* **178-179**, 45–54 (2016).
38. Azeem, M. et al. Optimal design of multilayer fog collectors. *ACS Appl. Mater. Interfaces* **12**, 7736–7743 (2020).
39. Nguyen, L. T. et al. Three-dimensional multilayer vertical filament meshes for enhancing efficiency in fog water harvesting. *ACS Omega* **6**, 3910–3920 (2021).
40. Montecinos, S., Carvajal, D., Cereceda, P. & Concha, M. Collection efficiency of fog events. *Atmos. Res.* **209**, 163–169 (2018).
41. Fernandez, D. M. et al. Fog water collection effectiveness: mesh intercomparisons. *Aerosol. Air Qual. Res.* **18**, 270–283 (2018).
42. Rivera, Jd. D. Aerodynamic collection efficiency of fog water collectors. *Atmos. Res.* **102**, 335–342 (2011).
43. Carvajal, D., Silva-Llanca, L., Larraguibel, D. & González, B. On the aerodynamic fog collection efficiency of fog water collectors via three-dimensional numerical simulations. *Atmos. Res.* **245**, 105123 (2020).
44. Langmuir, I. & Blodgett, K. B. *Collected Works of Irving Langmuir* (Pergamon Press, 2004).
45. Schemenauer, R. S. & Joe, P. I. The collection efficiency of a massive fog collector. *Atmos. Res.* **24**, 53–69 (1989).
46. Chen, H. et al. Ultrafast water harvesting and transport in hierarchical microchannels. *Nat. Mater.* **17**, 935–942 (2018).
47. Ojiako, C. J., Cimpeanu, R., Bandulasena, H. H., Smith, R. & Tseluiko, D. Deformation and dewetting of liquid films under gas jets. *J. Fluid Mech.* **905**, A18 (2020).
48. Wei, J., Xu, X., Zhang, J. & Liu, J. Measurement of liquid film coverage on vertical plates with hydrophilic and structured surface treatments. *Ind. Eng. Chem. Res.* **60**, 3736–3744 (2021).
49. Ledesma-Aguilar, R., Nistal, R., Hernandez-Machado, A. & Pagonabarraga, I. Controlled drop emission by wetting properties in driven liquid filaments. *Nat. Mater.* **10**, 367–371 (2011).
50. Quéré, D. Thin films flowing on vertical fibers. *Eur. Lett.* **13**, 721 (1990).
51. Kalliadasis, S. & Chang, H.-C. Drop formation during coating of vertical fibres. *J. Fluid Mech.* **261**, 135–168 (1994).
52. Duprat, C., Ruyer-Quil, C. & Giorgiutti-Dauphiné, F. Spatial evolution of a film flowing down a fiber. *Phys. Fluids* **21**, 042109 (2009).
53. Golovin, M. & Putnam, A. Inertial impaction on single elements. *Ind. Eng. Chem. Fundam.* **1**, 264 (1962).
54. Lamura, A., Gompper, G., Ihle, T. & Kroll, D. M. Multi-particle collision dynamics: Flow around a circular and a square cylinder. *Eur. Lett.* **56**, 319 (2001).
55. Haugen, N. E. L. & Kragset, S. Particle impaction on a cylinder in a crossflow as function of Stokes and Reynolds numbers. *J. Fluid Mech.* **661**, 239–261 (2010).
56. Brandon, D. J. & Aggarwal, S. K. A numerical investigation of particle deposition on a square cylinder placed in a channel flow. *Aerosol Sci. Technol.* **34**, 340–352 (2001).
57. Salmanzadeh, M., Rahnama, M. & Ahmadi, G. Particle transport and deposition in a duct flow with a rectangular obstruction. *Part. Sci. Technol.* **25**, 401–412 (2007).
58. Sau, A., Hsu, T.-W. & Ou, S.-H. Three-dimensional evolution of vortical structures and associated flow bifurcations in the wake of two side-by-side square cylinders. *Phys. Fluids* **19**, 084105 (2007).
59. Zheng, Q. & Alam, M. M. Intrinsic features of flow past three square prisms in side-by-side arrangement. *J. Fluid Mech.* **826**, 996–1033 (2017).
60. Boudina, M., Gosselin, F. P. & Étienne, S. Direct interception or inertial impaction? A theoretical derivation of the efficiency power law for a simple and practical definition of capture modes. *Phys. Fluids* **32**, 123603 (2020).
61. de la Mora, J. F. Inertia and interception in the deposition of particles from boundary layers. *Aerosol Sci. Technol.* **5**, 261–266 (1986).
62. Isobe, M. & Okumura, K. Initial rigid response and softening transition of highly stretchable kirigami sheet materials. *Sci. Rep.* **6**, 1–6 (2016).

63. Wood, R. & Loomis, A. L. XXXVIII. *The physical and biological effects of high-frequency sound-waves of great intensity. The Lond. Edinb. Dublin Philos. Mag. J. Sci.* **4**, 417–436 (1927).
64. Lang, R. J. Ultrasonic atomization of liquids. *J. Acoust. Soc. Am.* **34**, 6–8 (1962).
65. Kooij, S., Astefanei, A., Corthals, G. L. & Bonn, D. Size distributions of droplets produced by ultrasonic nebulizers. *Sci. Rep.* **9**, 6128 (2019).

ACKNOWLEDGEMENTS

This work was supported by the Fonds de la Recherche Scientifique—FNRS under Grant *n*° PDR-WISD-12.

AUTHOR CONTRIBUTIONS

P.-B.B., N.V. and D.T. designed the research work. A.C., P.-B.B. and D.T. designed and developed the experimental setup and the kirigami fog nets. P.-B.B. and D.T. acquired and analyzed the data. P.-B.B., F.W., N.V. and D.T. discussed and interpreted the results. N.D.C. developed a numerical tool to design and digitally fabricate the kirigami fog nets. P.-B.B. and D.T. wrote the main manuscript text. P.-B.B. prepared the figures. All authors reviewed the manuscript.

COMPETING INTERESTS

The authors declare no competing interests.

ADDITIONAL INFORMATION

Supplementary information The online version contains supplementary material available at https://doi.org/10.1038/s41545-023-00266-6.

Correspondence and requests for materials should be addressed to Pierre-Brice Bintein or Denis Terwagne.